

How do stratospheric perturbations influence North American weather regime predictions?

Article

Published Version

Creative Commons: Attribution 4.0 (CC-BY)

Open Access

Lee, S. H., Charlton-Perez, A. J. ORCID: <https://orcid.org/0000-0001-8179-6220>, Woolnough, S. J. ORCID: <https://orcid.org/0000-0003-0500-8514> and Furtado, J. C. (2022) How do stratospheric perturbations influence North American weather regime predictions? *Journal of Climate*, 35 (18). pp. 5915-5932. ISSN 1520-0442 doi: <https://doi.org/10.1175/JCLI-D-21-0413.1> Available at <https://centaur.reading.ac.uk/105242/>

It is advisable to refer to the publisher's version if you intend to cite from the work. See [Guidance on citing](#).

To link to this article DOI: <http://dx.doi.org/10.1175/JCLI-D-21-0413.1>

Publisher: American Meteorological Society

All outputs in CentAUR are protected by Intellectual Property Rights law, including copyright law. Copyright and IPR is retained by the creators or other copyright holders. Terms and conditions for use of this material are defined in the [End User Agreement](#).

www.reading.ac.uk/centaur

CentAUR

Central Archive at the University of Reading

Reading's research outputs online

How Do Stratospheric Perturbations Influence North American Weather Regime Predictions?

SIMON H. LEE,^a ANDREW J. CHARLTON-PEREZ,^a STEVEN J. WOOLNOUGH,^b AND JASON C. FURTADO^c

^a *Department of Meteorology, University of Reading, Reading, United Kingdom*

^b *National Centre for Atmospheric Science, Department of Meteorology, University of Reading, Reading, United Kingdom*

^c *School of Meteorology, University of Oklahoma, Norman, Oklahoma*

(Manuscript received 27 May 2021, in final form 8 May 2022)

ABSTRACT: Observational evidence shows changes to North American weather regime occurrence depending on the strength of the lower-stratospheric polar vortex. However, it is not yet clear how this occurs or to what extent an improved stratospheric forecast would change regime predictions. Here we analyze four North American regimes at 500 hPa, constructed in principal component (PC) space. We consider both the location of the regimes in PC space and the linear regression between each PC and the lower-stratospheric zonal-mean winds, yielding a theory of which regime transitions are likely to occur due to changes in the lower stratosphere. Using a set of OpenIFS simulations, we then test the effect of relaxing the polar stratosphere to ERA-Interim on subseasonal regime predictions. The model start dates are selected based on particularly poor subseasonal regime predictions in the European Centre for Medium-Range Weather Forecasts CY43R3 hindcasts. While the results show only a modest improvement to the number of accurate regime predictions, there is a substantial reduction in Euclidean distance error in PC space. The average movement of the forecasts within PC space is found to be consistent with expectation for moderate-to-large lower-stratospheric zonal wind perturbations. Overall, our results provide a framework for interpreting the stratospheric influence on North American regime behavior. The results can be applied to subseasonal forecasts to understand how stratospheric uncertainty may affect regime predictions, and to diagnose which regime forecast errors are likely to be related to stratospheric errors.

SIGNIFICANCE STATEMENT: Predicting the weather several weeks ahead is a major challenge with large potential benefits to society. The strength of the circulation more than 10 km above the Arctic during winter (i.e., the polar vortex) is one source of predictability. This study investigates how forecast error and uncertainty in the polar vortex can impact predictions of large-scale weather patterns called “regimes” over North America. Through statistical analysis of observations and experiments with a weather forecast model, we develop an understanding of which regime changes are more likely to be due to changes in the polar vortex. The results will help forecasters and researchers understand the contribution of the stratosphere to changes in weather patterns, and in assessing and improving weather forecast models.


KEYWORDS: Climate classification/regimes; North America; Stratosphere; Stratosphere-troposphere coupling; Subseasonal variability; Winter/cool season


1. Introduction

The framework of large-scale weather regimes is now increasingly used in wintertime subseasonal-to-seasonal (S2S) prediction (from ~2 weeks to 2 months ahead; White et al. 2017), although the concept of a weather “regime” is not new (Rex 1951). Regimes are characteristically recurrent, persistent,

and quasi-stationary (e.g., Michelangeli et al. 1995) with typical time scales of weeks, well suited to the subseasonal scale where they can manifest “windows of opportunity” for skillful extended-range forecasts (Mariotti et al. 2020; Robertson et al. 2020).

Unlike empirical orthogonal functions (EOFs) (e.g., Hannachi et al. 2007), regimes defined through clustering methods are not bound by orthogonality or variance partitioning constraints. These regimes can therefore more closely represent the full anomalous flow configuration on a given day by benefiting from “mode mixing” and are accordingly easier to interpret, providing a useful way to understand extended-range ensemble forecasts. By characterizing recurrent flow configurations, weather regimes can also be used to diagnose flow-dependent predictability (Ferranti et al. 2015; Matsueda

 Denotes content that is immediately available upon publication as open access.

 Supplemental information related to this paper is available at the Journals Online website: <https://doi.org/10.1175/JCLI-D-21-0413.1.s1>.

Simon H. Lee’s current affiliation: Department of Applied Physics and Applied Mathematics, Columbia University, New York, NY

Corresponding author: Simon H. Lee, simon.h.lee@columbia.edu



This article is licensed under a [Creative Commons Attribution 4.0 license](http://creativecommons.org/licenses/by/4.0/) (<http://creativecommons.org/licenses/by/4.0/>).

DOI: 10.1175/JCLI-D-21-0413.1

© 2022 American Meteorological Society. For information regarding reuse of this content and general copyright information, consult the [AMS Copyright Policy](https://www.ametsoc.org/PUBSReuseLicenses/) (www.ametsoc.org/PUBSReuseLicenses/).

and Palmer 2018). From an impacts perspective, regimes have been used to better understand meteorological impacts on energy demand (e.g., Grams et al. 2017; van der Wiel et al. 2019; Garrido-Perez et al. 2020), precipitation and wildfire risk (Robertson and Ghil 1999; Robertson et al. 2020), and public health (Charlton-Perez et al. 2019; Huang et al. 2020).

A significant source of tropospheric subseasonal predictability during boreal winter is variability in the Arctic stratospheric polar vortex, including sudden stratospheric warmings (SSWs; e.g., Charlton and Polvani 2007) and strong vortex events (e.g., Limpasuvan et al. 2005; Tripathi et al. 2015). The downward influence of the stratosphere can be viewed as the modulation of weather regime transition and persistence. Perhaps the simplest regime framework employs the two phases of the North Atlantic Oscillation (NAO), which are similar to the Northern Annular Mode (NAM) and Arctic Oscillation (AO) patterns and strongly influenced by the stratosphere (Ambaum et al. 2001; Baldwin and Thompson 2009; Hitchcock and Simpson 2014). More complex regime analyses for the North Atlantic–European sector invoke four (e.g., Vautour 1990; Cassou 2008), six (Falkena et al. 2020), or seven (e.g., Grams et al. 2017) regimes depending on the method, focus, or purpose of the analysis.

Using four North Atlantic regimes, Charlton-Perez et al. (2018) found significant differences in the occurrence likelihood of three regimes between strong and weak lower-stratospheric vortex states, while the probability of Scandinavian blocking was invariant. Beerli and Grams (2019) related the stratospheric modulation of Atlantic weather regimes to whether or not the regime projected strongly onto the NAO pattern. They emphasized that regimes that do not project strongly onto the NAO provide a route for a wider variety of weather patterns following anomalous stratospheric vortex states. Subsequently, Maycock et al. (2020) analyzed the North Atlantic response to SSWs from the perspective of modulation of the three eddy-driven jet regimes, finding an increase in the occurrence and persistence of the southernmost regime (corresponding to the negative NAO). Domeisen et al. (2020a) assessed the varying degrees of stratosphere–troposphere coupling following major SSWs (e.g., Karpechko et al. 2017; White et al. 2019) by considering the regimes present during SSW onset and in the weeks afterward, suggesting that the antecedent state of the troposphere may play an important role in determining subsequent downward coupling.

In recent years, the influence of the stratosphere on North American climate variability has received increased attention, likely owing to the extreme cold-air outbreaks during winter 2013/14 that accompanied disruption to the polar vortex (Yu and Zhang 2015; Waugh et al. 2017). However, relatively less attention has been given to explicitly viewing the impact of the stratosphere on North American weather from a tropospheric regimes perspective. As North America is influenced by weather from both the Atlantic and Pacific to different degrees across the continent, a challenge with defining North American regimes is the choice of domain. Some studies (e.g., Amini and Straus 2019; Fabiano et al. 2021) focus on upstream variability in the Pacific–North American (PNA) sector (akin to the Atlantic regimes with respect to Europe),

while others focus on the continent as a whole and incorporate both Atlantic and Pacific variability. Despite some methodological differences, a growing number of studies have defined a consistent and reproducible set of four wintertime regimes in the 500-hPa geopotential height anomaly field centered over North America (e.g., Straus et al. 2007; Vigaud et al. 2018; Lee et al. 2019b; Robertson et al. 2020). The regimes capture both PNA-like and NAO-like behavior.

More specifically, Lee et al. (2019b) analyzed these four North American regimes (the Arctic high, Arctic low, Alaskan ridge, and Pacific trough) in the context of the strength of the lower-stratospheric polar vortex in reanalysis. They found significant differences between the occurrence of three of the regimes during strong and weak stratospheric vortex states of a similar magnitude to those in Charlton-Perez et al. (2018) for the North Atlantic. The Alaskan ridge regime did not show a relationship with the stratospheric vortex strength, but was found to be strongly linked to North American cold waves. Lee et al. (2019b) hypothesized that tropical forcing (e.g., Wang et al. 2014) or stratospheric wave reflection (Kodera et al. 2016; Kretschmer et al. 2018; Matthias and Kretschmer 2020) may dominate driving the Alaskan ridge, owing to the similarity of the regime to patterns associated with both. As a purely observation-based study, the results of Lee et al. (2019b) were noncausal and did not assess when or how changes in the stratospheric state would change regime occurrence, or whether improved stratospheric forecasts would yield better regime predictions. Addressing these points is therefore a goal of the present study.

To diagnose the downward influence of the stratosphere on the troposphere, and changes in tropospheric forecast skill arising from a correctly predicted stratosphere, model experiments in which the stratospheric state is artificially nudged or relaxed to a different state (such as that from reanalysis) have been used. Most studies have focused on the seasonal-scale effects (Douville 2009; Hitchcock and Simpson 2014; Jung et al. 2010a,b). However, Kautz et al. (2020) used relaxation experiments on S2S time scales to quantify the role of the February 2018 SSW in the predictability and onset of the subsequent Eurasian cold wave. They found an increased probability of surface cold extremes in forecasts with a nudged stratosphere, but that the evolution of the lower-stratospheric NAM following the SSW—rather than simply the occurrence of the SSW—was important for more accurate tropospheric forecasts. The importance of persistent lower stratospheric anomalies in eliciting a tropospheric response is consistent with climate model studies (Maycock and Hitchcock 2015; Runde et al. 2016) and the polar-night jet oscillation events of Hitchcock et al. (2013).

Although SSWs and their strong vortex counterpart are typically harbingers of persistent anomalous lower-stratospheric NAM states (Baldwin and Dunkerton 2001), they do not necessarily propagate into the lowermost stratosphere, and anomalous lower-stratospheric NAM states can occur without a typical midstratospheric precursor. Hence, analysis of the effect of the stratosphere on the troposphere need not only focus on such extreme midstratospheric circulation events. Further, the NAM in the lower stratosphere during midwinter

possesses a very long time scale (over 4 weeks; Baldwin et al. 2003), key for the S2S prediction scale. In this study, we focus on subseasonal variability in the strength of the lower-stratospheric polar vortex, diagnosed through the zonal-mean zonal wind at 100 hPa and 60°N (U100). We do not explicitly consider SSWs or strong vortex events.

The overall goal of this study is to understand how changes or uncertainty in the subseasonal lower stratospheric vortex state can influence changes or uncertainty in predictions of North American weather regimes. We do this first by a statistical analysis of the regimes and their underlying EOFs in reanalysis, and then through analyzing a set of model experiments in which the stratosphere is nudged toward reanalysis. A greater understanding of the relationship between stratospheric variability and regimes will help in both the real-world understanding and interpretation of regime forecast uncertainty, and in subsequent studies of regime dynamics and predictability. It would also be a useful tool to examine how model biases affect the representation of stratosphere–troposphere coupling.

The paper is organized as follows. Section 2 introduces the data, methods, and model experiments. Section 3 defines the regimes and their underlying EOFs, and the relationship between these EOFs and the lower-stratospheric polar vortex strength. Section 4 develops a theory of how the stratosphere may influence regime behavior. Section 5 presents the results of a modeling study used to test the theory. A summary and conclusion of our work follows in section 6, including implications for S2S prediction.

2. Data and methods

a. Hindcasts and reanalysis

For historical analysis and verification, we use the European Centre for Medium-Range Weather Forecasts (ECMWF) ERA-Interim reanalysis (Dee et al. 2011). Hindcasts are taken from version CY43R3 of the ECMWF extended-range prediction system (used to produce operational forecasts from July 2017 to June 2018) as part of the S2S database. The hindcasts consist of an 11-member ensemble (1 unperturbed member and 10 perturbed members) initialized from ERA-Interim twice per week. The model has a resolution of Tco639¹ up to day 15 and Tco319 after day 15, and 91 vertical levels.² All data are sampled once per day at 0000 UTC, and regridded to 2.5° latitude–longitude resolution for computational efficiency and since we are only considering large-scale fields.

b. Regime definitions

The definition of North American weather regimes follows that of Lee et al. (2019b), extended by 1 year. We take 500-hPa geopotential heights (Z500) in the region 180°–30°W, 20°–80°N in all December–March days in the period 1 January 1979–31 December 2018 in ERA-Interim (4840 days) and subtract

the daily climatology over this period. (Any trends in Z500 are found to have little impact on the regimes, so detrending is not performed.) Then, data are weighted by the square root of cosine latitude, and EOF analysis is performed, retaining the leading 12 EOFs that explain close to 80% of the variance; *k*-means clustering is then performed (Pedregosa et al. 2011) in the non-standardized 12-dimensional principal component (PC) space, with *k* set to 4. In addition to reducing the dimensionality of the clustering problem and filtering smaller-scale variability, performing the clustering in PC space produces a coordinate system that enables interpretation of the regimes in terms of their comprising EOFs, linking two widely used prediction frameworks. After generating the clusters, each day is then assigned to one of the four regimes by the minimum Euclidean distance to the cluster centroids in PC space.

For regime assignment in the hindcasts, the model Z500 climate is first subtracted, to account for systematic biases. The model climate is computed for each initialization date and lead time over the 20-year hindcast period. Then, the daily data are projected onto the 12 EOFs, and each day is assigned to a regime based on these pseudo-PC loadings. As an additional forecast diagnostic in the model experiments, weekly mean regimes are produced by first averaging the PCs over a 7-day period and then assigning to a regime; these are found to be largely consistent with the regime occupying the majority of days within each week (not shown).

c. Regime bust criteria

We select subseasonal regime “busts” from the ECMWF hindcasts where there is strong ensemble support (≥ 7 members, or approximately two-thirds) for *one* specific incorrect regime to be dominant (i.e., present on at least 8 days) during days 14–27 (weeks 3–4). These criteria are designed to pick out cases that suggest a strong, but incorrect, subseasonal signal constraining the model analogous to a “precise but inaccurate” forecast. As such, the model confidence may be erroneously interpreted as enhanced predictability and accuracy, with potentially large real-world impacts from subsequent decision-making. We choose only hindcasts initialized during December–February, as the seasonal cycle may affect week-3–4 forecasts initialized during March. These criteria yield 31 initialization dates. A further stipulation is applied such that the initialization dates must be separated by at least 21 days to avoid analyzing multiple instances of the same event; in these cases, the earliest initialization date is selected. This step filters the number of cases to 20 (i.e., on average 1 per winter), which are listed in Table 1. Except for forecasts of an Arctic high verifying as an Alaskan ridge, all forecast–verification combinations are included at least once (not by design).

No stratospheric error criteria are included in order to assess both to what extent poor subseasonal regime forecasts are associated with stratospheric errors and the effect of stratospheric relaxation even in cases with a relatively well-forecast stratosphere. We find that the majority of bust cases feature ensemble-mean U100 error magnitudes $\geq 3 \text{ m s}^{-1}$ (14 of the 20 initialization dates, including 8 week-3 and 12 week-4 forecasts), approximately the mean absolute error

¹ Tco = cubic octahedral spectral truncation.

² Details of the prediction system can be found on the ECMWF website <https://confluence.ecmwf.int/display/S2S/ECMWF+Model>.

TABLE 1. North American regime busts in ECMWF CY43R3 hindcasts (HC) from December 1997 to February 2017. The week-3–4 dominant (W3–4 dom.) regime is that which is predicted by ≥ 7 ensemble members (64%) to be present on ≥ 8 days during days 14–27 inclusive, verified against the ERA-Interim regime that is present for ≥ 8 days during the same time period. Week-3 and week-4 regimes are the regimes of the weekly mean field with the largest ensemble support; εU is the ensemble-mean error in the 100-hPa 60°N zonal-mean zonal winds averaged over each week. The data are grouped by the dominant regime prediction and then sorted by the week-4 εU .

Initialization	W3–4 dom. percent (ERA)	W3 HC (ERA)	W3 εU (m s ⁻¹)	W4 HC (ERA)	W4 εU (m s ⁻¹)
Arctic high					
21 Dec 2005	64 (PT)	ArH (PT)	−0.5	ArH (PT)	4.2
1 Feb 2009	64 (ArL)	ArH (ArL)	2.5	ArH (ArL)	3.2
8 Feb 2010	73 (PT)	ArH (ArH)	0.3	ArH (PT)	−4.8
29 Jan 1998	64 (PT)	PT (PT)	−8.5	ArH (PT)	−6.7
Arctic low					
29 Jan 2001	73 (AkR)	ArL (ArL)	6.5	ArL (AkR)	8.5
28 Dec 2016	82 (AkR)	ArL (AkR)	2.7	ArL (AkR)	3.0
8 Feb 2006	64 (ArH)	ArL (ArH)	4.8	ArL (ArH)	2.3
22 Jan 1999	64 (PT)	ArL (PT)	−1.5	ArL (PT)	1.0
19 Feb 2011	64 (PT)	ArL (PT)	−0.3	ArL (PT)	−0.6
4 Dec 2011	64 (PT)	ArL (ArL)	0.1	ArL (PT)	−1.3
Alaskan ridge					
11 Dec 2001	64 (ArH)	AkR (ArH)	2.3	AkR (PT)	3.1
15 Feb 2017	64 (ArL)	AkR (ArL)	−0.6	AkR (AkR)	2.6
4 Dec 2003	73 (PT)	ArH (PT)	0.4	AkR (ArL)	−3.0
Pacific trough					
12 Feb 1999	64 (ArH)	PT (PT)	3.3	PT (ArH)	14.0
8 Jan 2010	64 (ArH)	PT (ArH)	4.1	ArH (ArH)	8.7
25 Dec 2015	73 (ArH)	PT (ArH)	7.7	PT (ArH)	7.7
7 Dec 2000	64 (ArH)	PT (ArH)	7.3	PT (ArH)	2.8
18 Jan 2016	73 (AkR)	PT (PT)	0.3	PT (AkR)	0.4
21 Dec 2014	73 (AkR)	AkR (AkR)	−1.7	PT (AkR)	−2.1
25 Dec 2006	82 (ArL)	PT (ArL)	−5.8	PT (ArL)	−8.7

(MAE) of the December–February week-3–4 hindcasts (see Fig. S1 in the online supplemental material). This suggests that regime busts and large lower-stratospheric vortex errors often co-occur.

d. OpenIFS model

For model experiments, we use OpenIFS³ version 43r3v1—a research version of the ECMWF IFS (Integrated Forecast System) model CY43R3, but without data assimilation. The model is initialized from ERA-Interim and run on a linear Gaussian grid with T255 resolution, 60 vertical levels (i.e., the resolution of ERA-Interim), and a time step of 45 min. Output data are bilinearly interpolated onto a 2.5° latitude–longitude grid. Each ensemble consists of an unperturbed member and 20 perturbed members, in which spread is generated by the stochastically perturbed parameterization tendencies (SPPT) and stochastic kinetic energy backscatter (SKEB) schemes (Leutbecher et al. 2017). The ensemble size is chosen as a balance between the potential gain from additional members compared with the 11-member hindcasts and computational expense. The OpenIFS runs differ from the operational model in both resolution and in that there is no

representation of initial condition uncertainty, so some differences between these model runs and the equivalent hindcasts are to be expected. As we are primarily considering forecasts on time scales of several weeks, the initial condition uncertainty is considered less important, and the stochastic schemes generate spread comparable to the hindcasts in the fields analyzed in this study.

For each initialization date, two sets of ensembles are produced: a control (CTR) run in which the forecast freely evolves (comparable with the equivalent hindcast, notwithstanding the model differences), and a relaxed (RLX) run in which the Arctic stratosphere is nudged toward ERA-Interim using the IFS relaxation scheme (e.g., Jung et al. 2010a). The relaxation scheme operates by applying a nonphysical tendency to the model equations of the form

$$\lambda(X_{\text{obs}} - X), \quad (1)$$

where X is a model prognostic variable, X_{obs} is the “observed” value from ERA-Interim, and λ [unit: (time step)⁻¹] is the relaxation coefficient controlling the strength of the forcing [following, e.g., Jeuken et al. (1996) and Magnusson (2017)]. The term X_{obs} at each model time step is generated by linear interpolation between 6-hourly reanalysis files. A relaxation time scale of 12 h is used in this study, corresponding to $\lambda = 0.0625$ per time step given the 45-min model time step, which can be interpreted

³ Specific details of the model can be found at <https://confluence.ecmwf.int/display/OIFS/Release+notes+for+OpenIFS+43r3v1>.

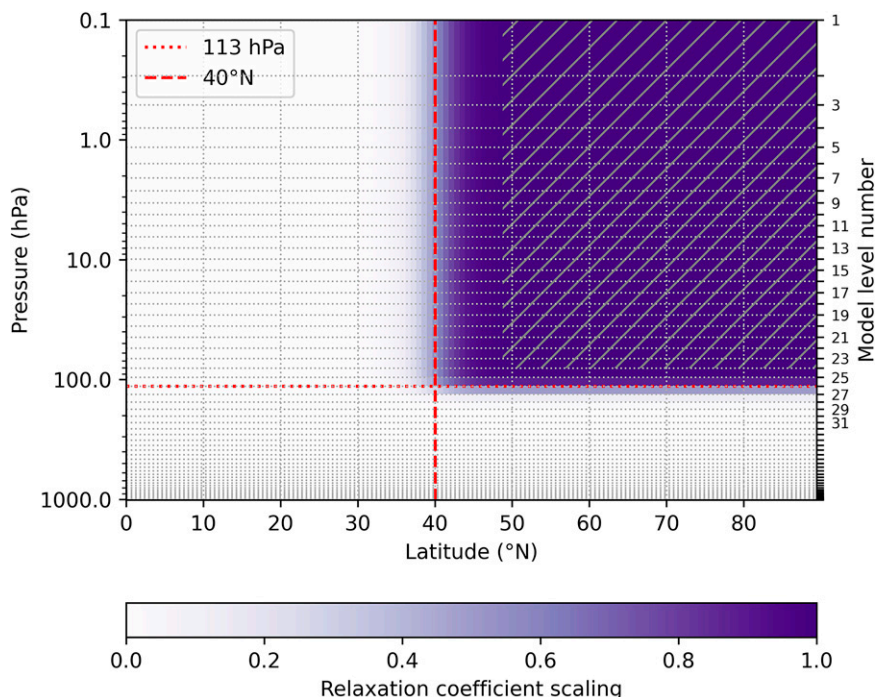


FIG. 1. Vertical and latitudinal profile of the relaxation coefficient scaling (i.e., a value of 1 denotes full relaxation, here with a time scale of 12 h), for both pressure (left-hand ordinate) and model level number (right-hand ordinate and horizontal grid lines; labeled to level 31 for clarity). The red dashed and dotted lines denote the bounds, in latitude and height respectively, where the coefficient is 0.5. The hatched area denotes the region where the scaling is at least 0.99.

as nudging the model state at each time step by 6.25% of the departure from the reanalysis. Vorticity, divergence, and temperature are relaxed in model gridpoint space with an exponential taper at both the latitude and model-level boundaries.

A profile of the relaxation domain is shown in Fig. 1. The domain boundaries are chosen to both maximize constraint of the polar lower stratosphere while allowing for a sufficiently smooth taper to minimize negative numerical effects, and to remain largely poleward and upward of the subtropical jet to reduce directly constraining the tropical upper-tropospheric waveguide. The choice of domain is also limited by the vertical level spacing of the model in the upper troposphere and lower stratosphere. We employ a weaker stratospheric nudging than some previous studies (e.g., Jung et al. 2010a; Kautz et al. 2020), but note that the relaxation in our study extends further into the lower stratosphere. Analysis of the output fields show this relaxation strength is enough to constrain the model. Time series of the U100 forecasts from the CTR and RLX experiments and the corresponding verification from ERA-Interim are shown in Fig. S2.

As the random seed used in the stochastic schemes is fixed for each ensemble member, the equivalent ensemble members in the CTR and RLX experiments differ only by the stratospheric nudging. In analyzing the OpenIFS runs, we assume the model climatology is equivalent to that of the corresponding CY43R3 hindcasts.

e. Significance testing

Throughout the paper, statistical significance is assessed at the 95% confidence level by bootstrap resampling (e.g., Wilks 2019). Random samples (with replacement) are taken from the population and the quantity under analysis (e.g., a regression coefficient) is calculated and stored. This process is repeated 10000 times, and then a confidence interval is constructed from the appropriate percentiles of this distribution (2.5th–97.5th percentiles for two-sided 95% confidence).

3. Regimes and EOFs

The centroids of the four regimes (expressed as the Z500 field reconstructed from the sum of the centroid loading in the leading 12 EOFs), along with the percent of days assigned to each (the occupation frequency), are shown in Figs. 2a–d. In terms of both spatial patterns and the ranking of occupation frequency, these match the regimes of Lee et al. (2019b) and so we follow their naming convention [after Straus et al. (2007)]: Arctic high (ArH), Arctic low (ArL), Alaskan ridge (AkR), and Pacific trough (PT). The coordinates of the regime centroids in the leading 12 PCs are shown in Fig. 2e. Only the leading three PCs have large contributions to the centroids; performing the same clustering analysis but retaining only the leading three PCs yields very similar patterns, with only 4% of days assigned to a different regime. Therefore, we now focus our analysis on these leading three EOFs.

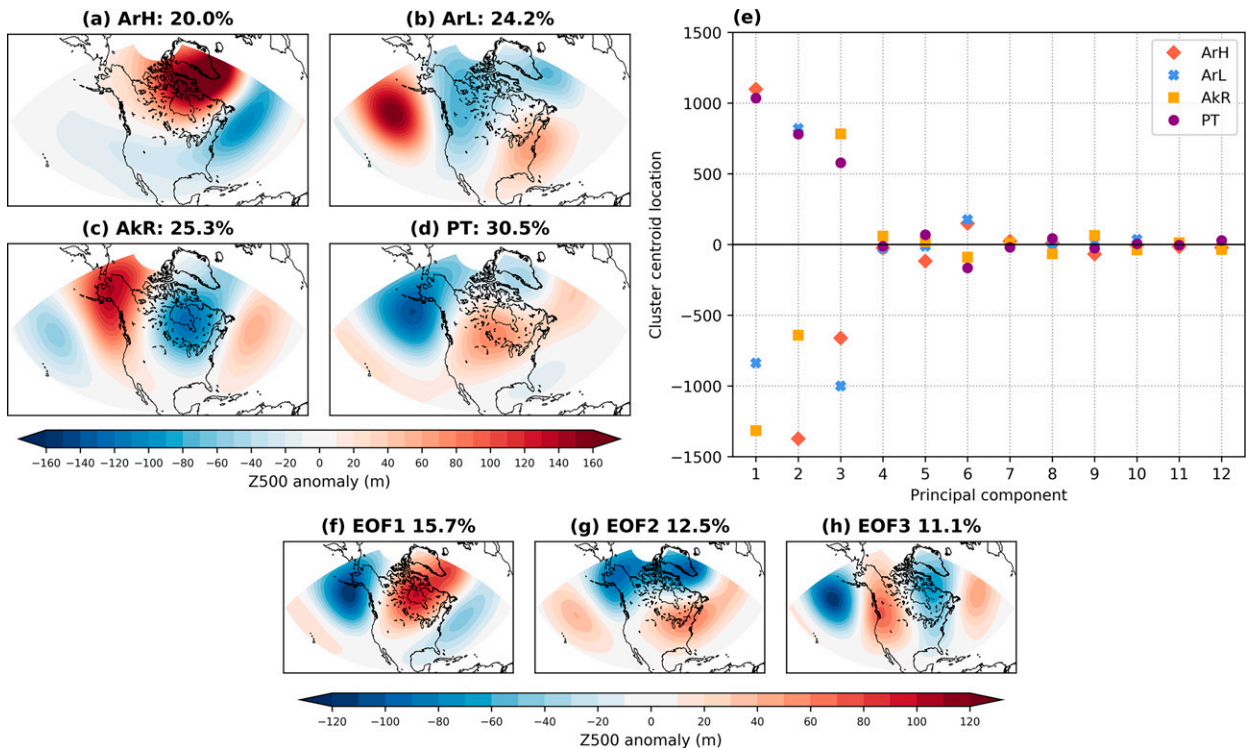


FIG. 2. (a)–(d) Centroids of the four regimes, expressed as 500-hPa geopotential height anomalies with respect to daily 1979–2018 climatology in ERA-Interim, and the percent of days assigned to each regime in all December–March days in the period 1 Jan 1979–31 Dec 2018. (e) Coordinates of the regime centroids in raw (nonstandardized) 12-dimensional principal component space. (f)–(h) The leading three EOFs (multiplied by the square root of the eigenvalue) of daily 500-hPa geopotential height anomalies in the domain 180° – 30° W, 20° – 80° N, and the percent of total variability explained by each EOF.

Maps of the EOFs and the percent of the total variance explained are shown in Figs. 2f–h. In total, these three EOFs explain close to 40% of the daily variance within the domain, and are well separated according to the criterion of North et al. (1982). The sign of the EOFs is here defined such that a positive loading produces an anomalous trough in the northeast Pacific. EOF1 is similar to the PNA (Wallace and Gutzler 1981) but slightly eastward shifted. It also bears some similarity to the tropical–Northern Hemisphere (TNH) pattern (Mo and Livezey 1986; Liang et al. 2017). Furthermore, there is a meridional dipole in the North Atlantic in the eastern edge of the domain, reminiscent of NAO-like variability. EOF2 has a meridional dipole in Z500 anomalies, and thus some similarity to the surface-based NAM/AO, but with a center of action over Alaska that is not characteristic of the surface NAM (e.g., Thompson and Wallace 1998). EOF3 is characterized by a wavenumber-2 pattern across the domain.

Comparison of these regional EOFs with the leading three EOFs for the Northern Hemisphere poleward of 20° N (Figs. S3–S5) shows a high degree of similarity in both the correlation of the PC time series (Pearson’s correlation $r \geq 0.77$; $p < 0.05$) and spatially (area-weighted pattern correlation ≥ 0.87 over the North American domain). We can therefore be confident that the leading three EOFs used in the clustering are regional manifestations of hemispheric variability, and that hemispheric variability is dominant in the smaller domain

under consideration. The EOFs presented here—with the most NAM-like pattern in EOF2, while the leading EOF contains NAM/NAO and PNA-like characteristics—agrees well with the upper-tropospheric EOF analysis of Baldwin and Thompson (2009). For all three North American EOFs, the e -folding time scales of the PC time series are 5–7 days, which is similar to the median number of consecutive days with the same regime assignment. However, a quarter of the individual blocks of consecutive regime days persist for more than 1 week (including one instance of 39 days of ArL up to and including 22 February 1990), motivating their utility for extended-range prediction.

To understand the relationship between regime occurrence and the lower-stratospheric vortex presented in Lee et al. (2019b), we examine the relationship between U100 and the leading EOFs which define the clusters. We perform linear regression between each PC time series and the contemporaneous U100 to see how changes in U100 may modulate the location of a point within the 3D PC space and thus its regime attribution. The instantaneous relationship is used since we are considering the lower stratosphere as an upper boundary condition to the troposphere, with both a much longer memory (e.g., Baldwin et al. 2003) and greater predictability (Son et al. 2020); lagged relationships (not shown) reveal these coefficients are either effectively maximized at lag 0 or, considering uncertainty, largely invariant for ± 7 days (within the

PC e -folding time scale). Some of this relationship may relate to the vertical extension of a primarily tropospheric zonal wind signature associated with these EOFs into the lower stratosphere. However, on subseasonal scales (well beyond tropospheric decorrelation time scales) this remains the component of the structure that is potentially predictable.

The regression coefficients are shown in Fig. 3. Although the coefficients for all three EOFs are significantly different from zero, the linear relationship is 3–5 times stronger for EOF2. Similarly, the Pearson's correlations between U100 and PCs 1 and 3 are small ($r = -0.13$ and 0.10 , respectively), but moderate for PC2 ($r = 0.42$). Thus, the effect of the stratosphere in this 3D EOF space is mostly contained within EOF2, which is consistent with its annular-like spatial pattern and the height-dependent NAM results of Baldwin and Thompson (2009). The sign of the regression coefficients is such that a decrease in U100 is associated with an increase in Z500 in the vicinity of Greenland/the northern node of the NAO, in agreement with the canonical response of the troposphere to a weakened stratospheric vortex.

4. Theory of regime transitions and the stratosphere

In this section, we develop a theory of which regime transitions may be possible solely due to a stratospheric perturbation by jointly considering the linear relationship between U100 and the three PCs, and the location of the regimes within the space spanned by the three PCs. The theory can be interpreted as an idealized framework where all else is instantaneously equal and only the stratosphere is changed, retaining potential predictability arising from other tropospheric processes.

Using the regression coefficients between U100 and the PC time series, we define the stratospheric perturbation vector β . This vector represents the movement within the 3D PC space arising from a perturbation to U100, ΔU , that is explained by the linear regression coefficients:

$$\beta = \Delta U \begin{pmatrix} -32 \\ 91 \\ 20 \end{pmatrix}. \quad (2)$$

Note that β is not a function of the position within PC space and is thus constant for a given ΔU . While the truncation to a 3D PC space was earlier motivated by the coordinates of the regime centroids, the linear relationship between the leading three EOFs and U100 also accounts for nearly all of the linear relationship with Z500 (Fig. S6).

The transition vector γ between two points (e.g., two cluster centroids) within this space is then defined as the respective distances between the coordinates in the three PCs:

$$\gamma = \begin{pmatrix} \Delta PC_1 \\ \Delta PC_2 \\ \Delta PC_3 \end{pmatrix}, \quad (3)$$

where $\Delta PC_k = PC_k(B) - PC_k(A)$ for the transition from point A to point B . Hence, inverse transitions have an equal but opposite transition vector: $\gamma(A, B) = \gamma(B, A)$.

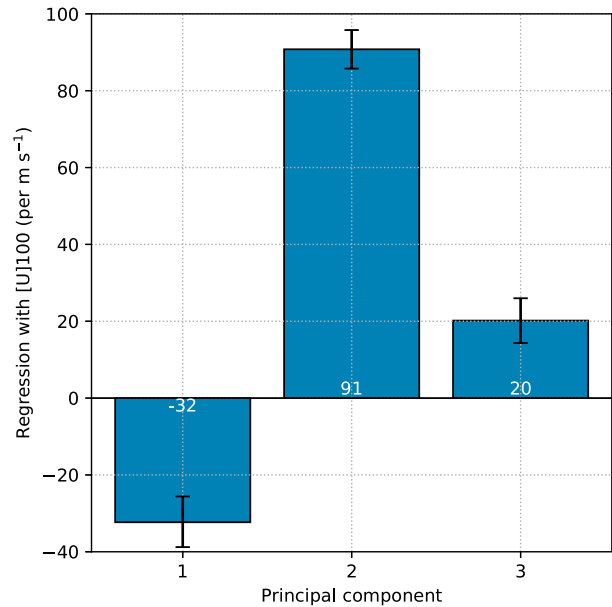


FIG. 3. Linear regression coefficients between the 100-hPa 60°N zonal-mean zonal wind and the raw PC time series of the leading three EOFs, in all December–March days in ERA-Interim 1979–2018. Error bars indicate 95% confidence intervals obtained by bootstrapping with replacement (see section 2e for details).

The angle θ between β and γ follows as

$$\theta(\beta, \gamma) = \arccos\left(\frac{\beta \cdot \gamma}{\|\beta\| \|\gamma\|}\right), \quad (4)$$

where $\|\mathbf{x}\| = \sqrt{x_1^2 + x_2^2 + x_3^2}$ denotes the Euclidean norm of a 3D vector \mathbf{x} .

We use this framework to model which regime transitions are possible solely with stratospheric forcing by considering whether the vectors β (either positive or negative) and γ point in a similar direction, known as “cosine similarity” (e.g., Han et al. 2012). If $\theta \geq 90^\circ$ ($\cos\theta \leq 0$), then no component of the regime transition or movement within the 3D PC space can be explained by the linear relationship between the PCs and U100, since the contribution of β would be 0 (in the case of maximally dissimilar vectors, $\theta = 90^\circ$) or oppose γ ($\cos\theta < 0$). A smaller angle indicates the transition is more likely since the projection of β in the direction of γ is larger (as $\cos\theta$ is larger), thus requiring a smaller ΔU . We focus on angles, rather than explicit distances, since the distances between regimes for any point are dependent on the initial location.

Figure 4 presents a 3D depiction (in the space spanned by the leading three EOFs) of β (both positive and negative; i.e., for a strengthening or weakening stratospheric vortex) applied to each regime centroid and the transition vector γ between the centroids. The regime centroids form a tetrahedron in this space. Some of the transition vectors lie closer to β than others owing to their relative locations within this space. For example, the positive β vector and the transition vector from the ArH to PT centroids are close, while the transition vectors from the AkR centroid are almost perpendicular to either sign of β .

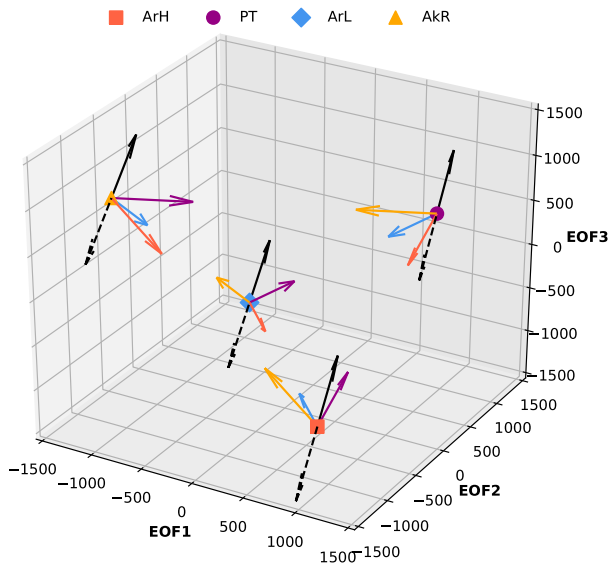


FIG. 4. Visualization of the regimes in the space occupied by the leading three EOFs. Colored markers indicate the regime centroids. Colored arrows represent the transition vectors from each centroid to the other centroids, scaled to $0.25\times$. The black arrows show the stratospheric perturbation vector, scaled to a $\pm 10 \text{ m s}^{-1}$ perturbation (solid positive; dashed negative), which is the same at all points.

The angles between the centroid γ vectors and β are quantified in the protractor-like polar plots in Fig. 5. The angles are expressed such that both positive and negative β are aligned with 0° (thus, the angle between each γ and $\beta < 0$ is a reflection of that to $\beta > 0$ about 90°). For a point starting at the ArH centroid (Fig. 5a), there is substantial cosine similarity between $\beta > 0$ and transition vectors to *all* other regimes (for all three, $\theta < 60^\circ$). The similarity is strongest for the transition vectors to PT and ArL, which have approximately equal cosine similarity. The angles between $\beta < 0$ and all three transition vectors are $> 90^\circ$; thus, the theory does not allow a transition away from ArH given $\Delta U < 0$. Overall, ArH has the largest number of transition vectors with small angles/high cosine similarity. Equally, the minimum angle between either sign of β and any γ vector is between $\beta < 0$ and transitions to ArH (Figs. 5b–d). This is consistent with the observed probability of transitions into, and the persistence of, ArH/NAO-, which is the most sensitive of both the North American and North Atlantic regimes to the strength of U100 (Charlton-Perez et al. 2018; Lee et al. 2019b).

For the PT regime (Fig. 5b), there is a small angle between the negative β vector and the transition vector to ArH (i.e., equal and opposite to the positive β and the transition from ArH to PT). While transitions are possible to both AkR with $\beta < 0$, and to ArL with $\beta > 0$, the angles are close to 90° , suggesting that these are unlikely. Considering the ArL regime (Fig. 5c), transitions to all three other regimes are possible with $\beta < 0$. The smallest angle is to the ArH transition vector, while the angles to the PT and AkR transitions are large. No regime transitions from ArL are possible in this framework with $\Delta U > 0$. Last, the angles between the transition vectors

and β are all relatively large for AkR (Fig. 5c), as previously suggested by the 3D depiction in Fig. 4. For $\beta < 0$, only a transition to ArH has an angle $< 90^\circ$. Transitions to ArL and PT are possible with $\beta > 0$, but the angles are relatively large and thus more unlikely.

We next extend our analysis beyond points initiating at the centroids and incorporate the effect of spread around the PC space spanned by each regime. First, we consider all the assigned regime days in ERA-Interim. The leading three PCs are then perturbed by β in the range $-30 \leq \Delta U \leq 30 \text{ m s}^{-1}$, and subsequently reassigned to a regime by minimum Euclidean distance. The maximum magnitude of ΔU is chosen here to be close to the maximum observed variability in U100; the largest U100 errors in individual CY43R3 ensemble members are close to $\pm 20 \text{ m s}^{-1}$. Note that in reality, the tropospheric response may be larger for a smaller ΔU as a consequence of the linear framework.

Figure 6 depicts the conditional probability, for each initial regime, of either remaining in the same regime or transitioning to each of the other regimes for each ΔU . Only those transition pathways with $\theta < 90^\circ$ occur, and the relative likelihood manifests the degree of similarity (i.e., the angle) between β and γ . There are no transitions away from ArH for $\Delta U < 0$ (Fig. 6a) or away from ArL for $\Delta U > 0$ (Fig. 6c). For $\Delta U < 0$, the dominant transition for all regimes is to ArH. For $\Delta U > 0$, transitions from ArH to PT dominate (Fig. 6a) while transitions to ArL dominate for AkR and PT (Figs. 6b,d). Transitioning into AkR from any other regime is unlikely even for large $|\Delta U|$, while transitioning out of AkR is the least likely for any of the regimes where a transition pathway exists (despite its unique approximately equal sensitivity for either sign of ΔU). Although not explicitly shown, there is also evidence of multiple transitions occurring as $|\Delta U|$ increases. For example, the probability of transitioning into AkR from each of the other regimes reaches a peak for $|\Delta U|$ between 10 and 20 m s^{-1} before declining.

As a general diagnostic of the sensitivity of each initial regime state to a lower-stratospheric perturbation, we can consider the probability of transitioning out of the regime for $\Delta U = \pm 10 \text{ m s}^{-1}$ (approximately equal to the maximum week-3–4 ensemble-mean U100 error magnitude in CY43R3 hindcasts). For $\Delta U = 10 \text{ m s}^{-1}$, 58% of ArH days transition into a new regime, while only 17% of AkR days and 6% of PT days do so. For $\Delta U = -10 \text{ m s}^{-1}$, the sensitivity of PT and ArL is approximately equal, with 39% of PT and 38% of ArL days transitioning into a new regime. Only 15% of AkR days transition into a new regime.

Overall, the results presented in Figs. 4–6 are in agreement with the observed differences in regime occurrence in strong and weak stratospheric vortex states in Lee et al. (2019b). The theory also gives results consistent with the relationship between the regimes (particularly ArH and ArL) and the concurrent NAO index (Fig. S7), given the strong modulation of the NAO by the stratosphere. Further, the proposed framework yields insight into specific regime transitions under different vortex states that are not limited by the observational sample size. In summary:

- $\Delta U < 0$ moves the majority of points within PC space toward *only* ArH, consistent with this regime being the *only* one more likely under weak vortex conditions.

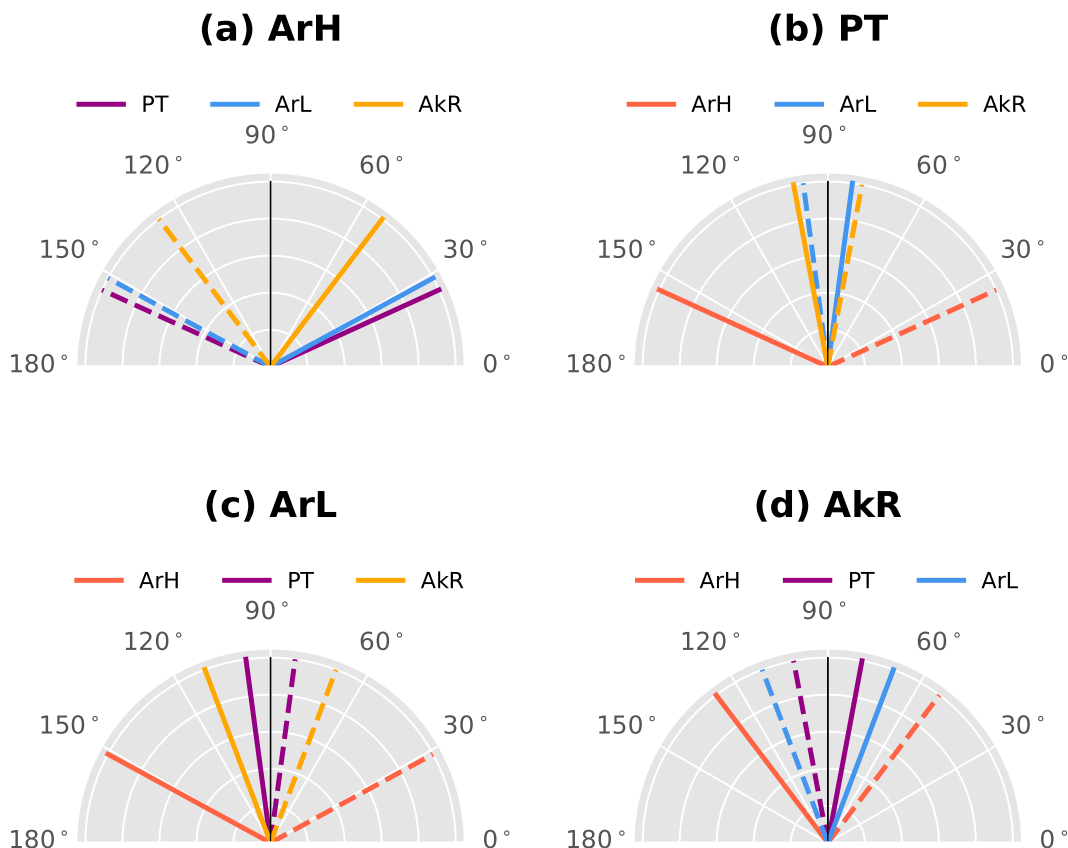


FIG. 5. Polar plots showing angles between the stratospheric perturbation vector (solid positive; dashed negative) and the centroid transition vector for each of the four regimes in 3D EOF space, as visualized in Fig. 4.

- $\Delta U > 0$ does little to changing the regime assignment for days initially assigned to ArL or PT, while these are favored transitions for initial ArH and AkR states. This is consistent with ArL and PT being more likely under strong vortex conditions.
- Very large ΔU is required to shift toward and away from AkR, with a similar proportion of transitions resulting from both positive and negative perturbations. This behavior is consistent with the observed statistically equal occurrence of this regime in strong and weak vortex states.

These conclusions are highly idealized, requiring both a perfectly linear response and the sole (or dominant) change being to U100. It is also possible that β may be sensitive to the initial position within PC space. However, the corroboration with observations suggests the potential use of this framework in interpreting the regime response to changes and uncertainty in the stratosphere on subseasonal time scales. The analysis in the next section considers whether imposing stratospheric relaxation yields a tropospheric response consistent with this simple but novel theory.

5. Model experiments

In analyzing the results of the relaxation experiments, we seek to answer the following two questions:

- What is the effect of stratospheric relaxation on regime forecast accuracy in these cases?
- Regardless of the forecast accuracy, is the change in the forecast consistent with the theory in section 4?

a. Regime predictions

A comparison between the weekly mean regimes in the CTR and RLX ensembles, for weeks 3 and 4, is shown in Fig. 7. The improvement in the total number of ensemble members with a correctly assigned weekly mean regime is modest: 13% in week 3 and 15% in week 4. Therefore (recalling that these cases were selected as particularly poor forecasts), the overall fraction of correctly assigned regimes remains low in the RLX experiment: 40% in week 3 and 25% in week 4. Any improvement is also case dependent. The greatest improvement in week 3 is in the 11 December 2001 case (7 more members correctly assigned to ArH), and in the 29 January 1998 case (5 more members correctly assigned to PT) in week 4. The latter was a case with a very large U100 error (cf. Table 1). In several cases, there is a decrease in the number of correctly assigned ensemble members. Thus, constraining the stratospheric state is not enough to fix these regime bust cases—which may be unsurprising given that only a selection of these cases have very large stratospheric errors, while all have largely inaccurate regime predictions. This result indicates that the stratospheric state should not be viewed

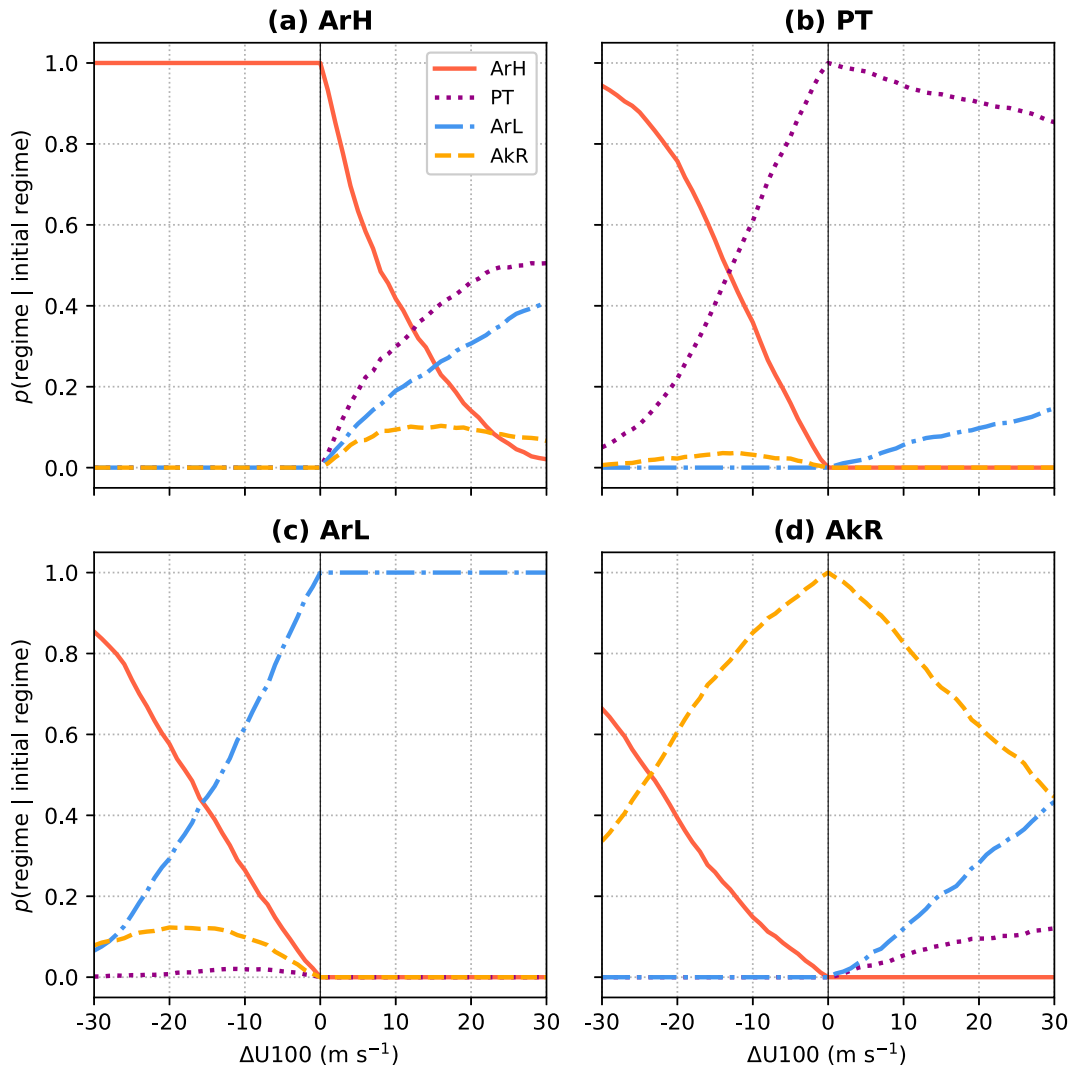


FIG. 6. (a)–(d) Given each initial regime, the conditional probability of either remaining in the same regime or transitioning to each of the other regimes, when all days assigned to each regime in ERA-Interim are perturbed by the stratospheric perturbation vector in the range $-30 \leq \Delta U \leq 30 \text{ m s}^{-1}$.

as exerting simple *control* on the subseasonal tropospheric flow over North America.

Figure 7 also shows that there are changes to the number of ensemble members assigned to the *incorrect* regimes, regardless of whether there is a change to the number assigned to the correct regime. On a member-by-member basis, 34% and 57% of the total ensemble members in weeks 3 and 4 respectively are assigned to a different regime in the RLX experiments. Thus, by week 4, the stratospheric nudging has shifted the majority of ensemble members into a new regime—suggesting significant movement within the PC space in which the regimes are assigned. For example, in week 4 of the 11 December 2001 case, there is no increase in the number of members correctly assigned to PT, but there is a gain of eight ensemble members assigned to AkR (with ArH and ArL losing four members each). While a full case-by-case analysis may yield further specific insight, it is beyond the scope of this

study; we instead focus on the general results across this set of forecasts.

b. Error reduction in PC space

Despite the small and case-dependent regime improvement, for almost all cases the mean Euclidean distance error of the ensemble in 3D PC space is reduced (Fig. 8a). This diagnostic is useful because it incorporates changes to forecasts that maintain the same regime attribution and is proportional to the root-mean square error (RMSE) of the Z500 field reconstructed from the leading three EOFs (see the online supplemental material; note that because non-normalized PCs are used, the total error on subseasonal time scales is dominated by the EOFs with the largest eigenvalues). Hence, in the space in which regimes are assigned, the RLX forecasts are almost entirely closer to the verification. The improvement is maximized in week 3 (median 14%), with only two

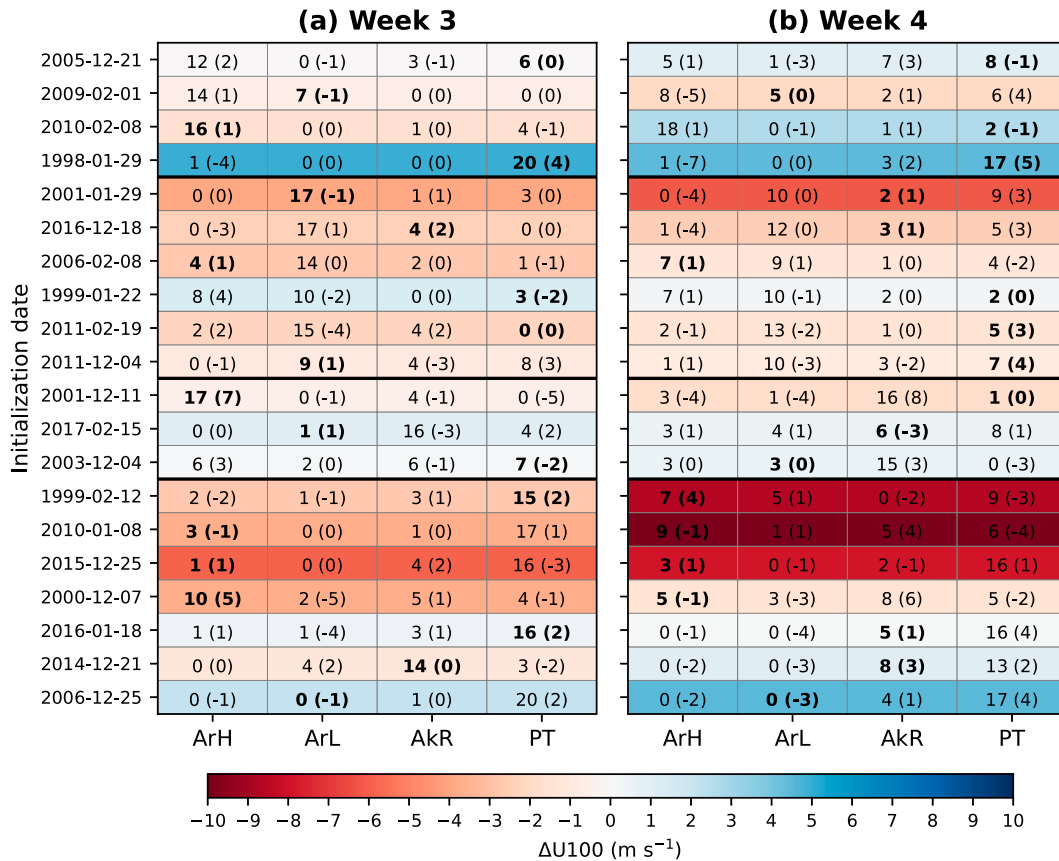


FIG. 7. For (a) week 3 and (b) week 4, values denote the number of ensemble members assigned to each regime in the RLX experiment, with the number in parentheses indicating the difference from CTR. Bold font indicates the ERA-Interim regime. Color shading indicates the difference in ensemble-mean U100 between the experiments (RLX-CTR). Grouping is as in Table 1.

cases showing an increase in error (21 December 2005 and 8 February 2010, both of which had negligible week-3 U100 errors in the CTR run). The median improvement in week 4 is 12%, but with much greater spread than week 3. There was a 30% improvement in a single case (21 December 2014), while four cases show no change or increased error (7 December 2000, 11 December 2001, 8 February 2010, and 15 February 2017).

Also shown in Fig. 8a is the mean change in Euclidean distance error obtained by perturbing the PCs of the CTR ensemble by β multiplied by ΔU between the CTR and RLX experiments. This shows that a simple statistical nudge of the PCs using the known linear relationships also yields an error reduction of on average $\sim 50\%$ of that obtained by running the full dynamical relaxation experiment. Thus, a substantial component of the dynamical effect of imposing a different stratospheric state on these EOFs can be explained by the observed linear relationship between the PCs and U100.

To understand whether larger stratospheric forcing yields larger error reduction, Fig. 8b shows the case-by-case change in ensemble-mean Euclidean distance error against the magnitude of the U100 change between the CTR and RLX experiments for weeks 3 and 4. There is no immediately clear relationship, with the greatest error reduction occurring with

a U100 change of only 1 m s^{-1} while the largest error increase occurs with a U100 change of 2.6 m s^{-1} (8 February 2010). The large relative error reduction for small ΔU suggests a potential role of zonally asymmetric corrections or other changes to the vortex that do not project strongly onto U100 (and thus fall outside the framework proposed here). However, across this set of 20 cases, for ΔU exceeding 3 m s^{-1} , there is a systematic error reduction. We revisit this apparent threshold in the analysis below.

c. Movement within PC space

We now investigate whether the movement of the forecasts within 3D PC space is consistent with what might be expected from the theory established in section 4. For this analysis, we analyze three vectors and three different angles within PC space. Figure 9 shows a schematic of this approach. The vectors are defined as follows:

- CTR-ERA: the vector between the CTR forecast and the verification from ERA-Interim (i.e., the error in the CTR forecast).
- CTR-RLX: the vector between the CTR and RLX forecasts.

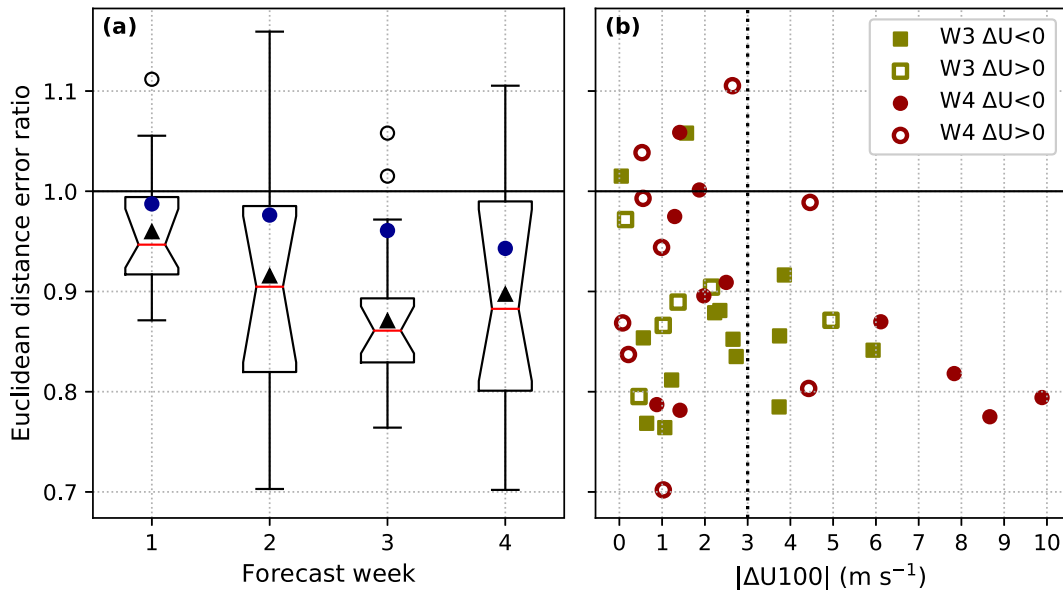


FIG. 8. (a) Boxplots of the ratio between the ensemble-mean Euclidean distance error in 3D PC space between the weekly averaged RLX and CTR ensembles for the 20 cases. Red lines denote the median, and notches show 95% confidence intervals obtained by 10 000 bootstrap resamples (with replacement). Black triangles denote the mean. Blue circles represent the average ratio obtained by statistically perturbing the CTR PCs by the stratospheric perturbation vector multiplied by the change in U100 between the CTR and RLX ensembles. Whiskers extend to 1.5 times the interquartile range or extremes (whichever is smaller); outliers shown as open circles. (b) Scatterplot of the week-3 (green squares) and week-4 (maroon circles) error ratio against the magnitude of the ensemble-mean change in U100 between CTR and RLX.

- CTR-STAT: the vector between the CTR forecast and the CTR forecast statistically perturbed by β multiplied by ΔU between CTR and RLX ensembles (STAT).

Then, the size of the three angles can be used to answer the following questions:

- $\theta_1 = \theta(\text{CTR-ERA}, \text{CTR-RLX})$: Does stratospheric relaxation move the CTR forecast toward the verification?
- $\theta_2 = \theta(\text{CTR-RLX}, \text{CTR-STAT})$: Does stratospheric relaxation move the CTR forecast in the direction expected from β ?
- $\theta_3 = \theta(\text{CTR-ERA}, \text{CTR-STAT})$: Does statistical nudging by β move the CTR forecast toward the verification?

A scatter of the week-3 and week-4 angles versus the magnitude of ΔU between the CTR and RLX experiments is shown in Fig. 10. To focus on the overall shift of the ensemble in the relaxed experiments, and since β is defined from linear best-fit regression coefficients, we perform this analysis on the perturbations to the PCs and U100 averaged across the ensemble. Nevertheless, similar results are obtained when considering the results across all individual ensemble members (not shown). Figure 10a shows that in the majority of cases and in both weeks 3 and 4, the stratospheric relaxation generally moved the predictions toward the verification. Only two cases in week 3 and six cases in week 4 do not exhibit any similarity (i.e., $\theta > 90^\circ$). These results are consistent with the reduction in Euclidean distance error and its relationship with the magnitude of ΔU (Fig. 8).

Figure 10b assesses whether the stratospheric perturbation vector outlined in section 4 is a good representation of the effect of a dynamically applied stratospheric perturbation. For $|\Delta U| < \sim 3 \text{ m s}^{-1}$, the points are scattered across almost the full range of angles, indicating no clear relationship between the theory and the movement of these forecasts in PC space. However, although the sample is smaller, for $|\Delta U| > \sim 3 \text{ m s}^{-1}$, the angles are systematically much smaller than 90° —especially for week-4 forecasts, which feature larger ΔU . Hence, we conclude that on average, these forecasts moved in PC space in the general direction expected from the theory.

Finally, Fig. 10c assesses whether the simple statistical perturbation moves the CTR forecast toward the verification without running a full dynamical experiment (cf. Fig. 10a). As in Fig. 10b, but unlike in Fig. 10a, there is no clear evidence of vector similarity for small ΔU , but there is evidence of a systematic shift for ΔU exceeding $\sim 3 \text{ m s}^{-1}$ in magnitude. As a result, for larger U100 errors the tropospheric forecast can be partially corrected statistically (as indicated by Fig. 8a), but there is evidently additional gain from a dynamically corrected stratosphere even for small ΔU .

The 3 m s^{-1} threshold is most apparent for angles involving β , although there is some suggestion for the behavior of the RLX experiment (in terms of both angles and Euclidean distance error). It is not clear why 3 m s^{-1} should be a threshold; it may be related to the signal magnitude required to emerge above the typical ensemble-mean variability, and thus may be sensitive to ensemble size. Across the CY43R3 hindcasts,

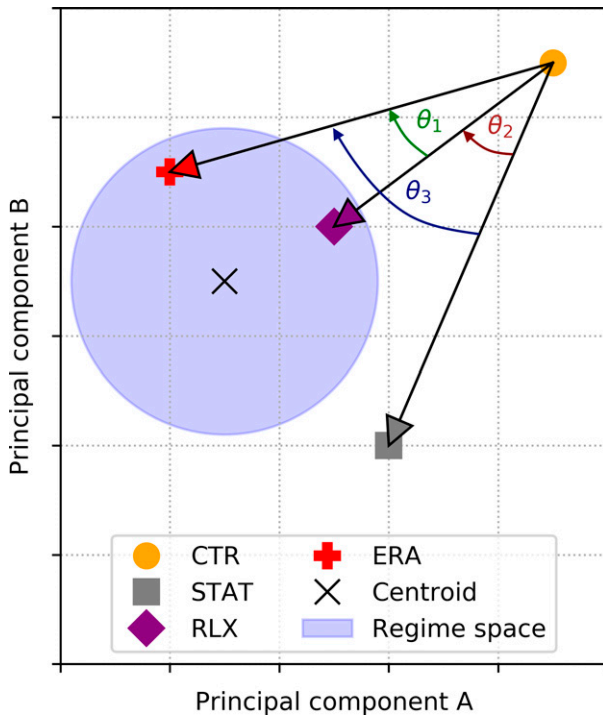


FIG. 9. Schematic of the angle-based approach (here in a 2D PC space). There are three vectors: the vector from the control forecast to the ERA-I verification (CTR-ERA; red), the vector from the control forecast to the relaxed forecast (CTR-RLX; purple), and the stratospheric perturbation vector to the statistically nudged forecast (CTR-STAT; gray). Here θ_1 denotes the angle between CTR-ERA and CTR-RLX, θ_2 the angle between CTR-RLX and CTR-STAT, and θ_3 the angle between CTR-ERA and CTR-STAT.

3 m s^{-1} is approximately two-thirds of the standard deviation of the ensemble-mean U100 in weeks 3–4 ($\sim 4.5 \text{ m s}^{-1}$), although these are not directly comparable owing to the smaller hindcast ensemble size. As mentioned in section 2, 3 m s^{-1} is also approximately the MAE of the ensemble-mean week-3–4 U100 in the CY43R3 hindcasts, and so errors of this magnitude are a reasonably frequent occurrence.

In week 4 (when ΔU is generally largest), the magnitude of the correlations between the ensemble-mean change in the PCs and the ensemble-mean ΔU from CTR to RLX (and thus the individual components of β) are maximized. These correlations are largest for EOF2 ($r = 0.60$, $p < 0.05$) and EOF3 ($r = 0.48$, $p < 0.05$) but the correlation is small and insignificant for EOF1 ($r = -0.19$, $p = 0.40$; although it is similar to that in ERA-Interim). Furthermore, we can find the “effective” vector in the model by computing the regression coefficients between ΔU and each ΔPC across all ensemble members. For weeks 3–4, these are not significantly different from the components of β in ERA-Interim, except slightly for EOF1 in week 3. As a result, the angles between this effective vector and β are small (26° in the week-3 forecasts and 12° in the week-4 forecasts), confirming that β is a good approximation of the response to an imposed stratospheric change.

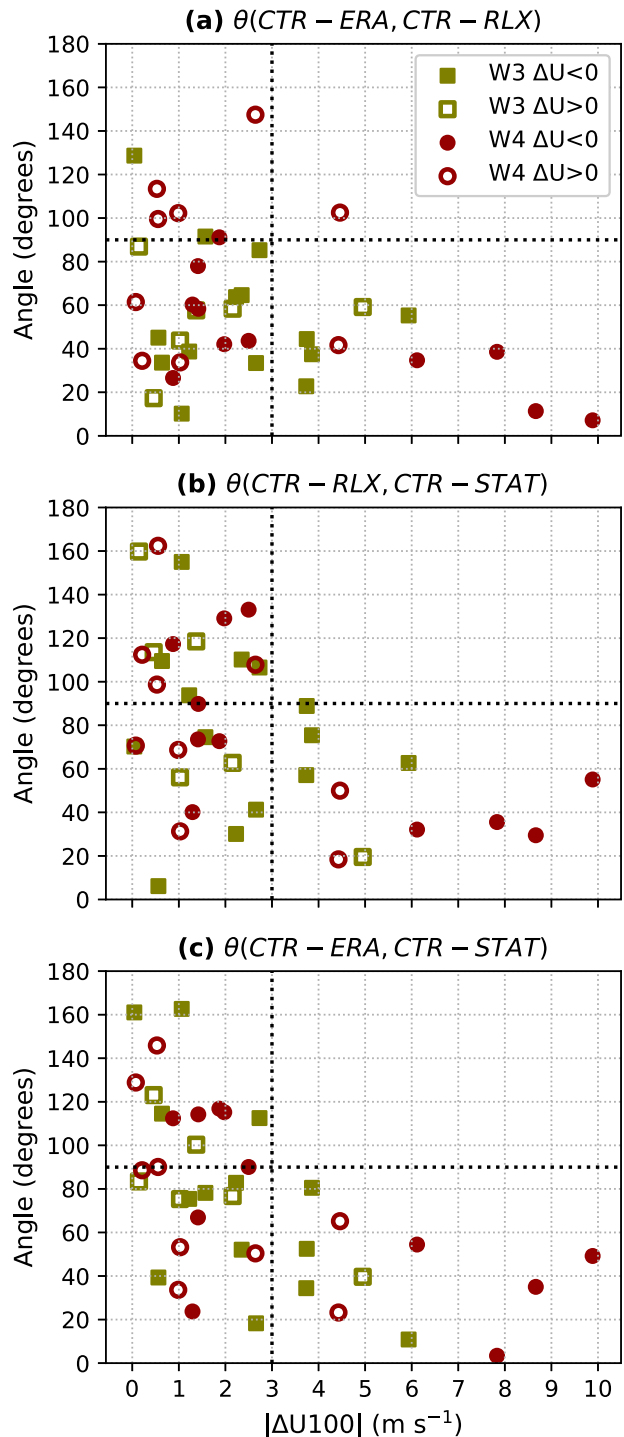


FIG. 10. Scatterplots of the magnitude of the ensemble-mean weekly mean U100 change between the CTR and RLX experiments, vs the angle between (a) CTR-ERA and CTR-RLX (θ_1), (b) CTR-RLX and CTR-STAT (θ_2), and (c) CTR-ERA and CTR-STAT (θ_3), in 3D-PC space.

Nevertheless, across the range of cases studied here, the response of EOF1 to stratospheric perturbations is not well approximated by linear regression. This may be due to nonlinearity, or that the relationship between the EOF and U100 is not causal (recalling the similarity between the EOF and patterns related to tropical forcing). Sample size may be an issue, given that the small expected response in EOF1. There may also be limitations in the representation of stratosphere–troposphere coupling in the model, such as the overestimation of the NAO response reported by Kolstad et al. (2020) using a similar but more recent ECMWF forecast model (CY45R1). The relatively low vertical resolution employed here, particularly in the upper troposphere and lower stratosphere, may also have limited the downward coupling and forecast improvement arising from the stratosphere (Kawatani et al. 2019; Domeisen et al. 2020c).

6. Summary and conclusions

Understanding and exploiting stratospheric variability is a key way in which the accuracy and usefulness of S2S forecasts and the fidelity of stratosphere–troposphere coupling within models can be increased. In this study, we investigated how perturbations to the strength of the lower-stratospheric polar vortex can influence North American weather regime predictions. Our novel technique involved jointly considering the linear relationship between the vortex strength and the leading EOFs that contribute to the regimes (Fig. 3), and the relative location of the regimes within the EOF space (Fig. 4). We used an angle-based approach to quantify which transitions are likely to occur (using cosine similarity) for a given regime and stratospheric perturbation (Fig. 5). These results agree with the observed changes in regime occurrence under different stratospheric vortex states reported in Lee et al. (2019b) and provide an explanation for the regime behavior. However, both the regime framework and EOFs are defined primarily from a mathematical, rather than physical, standpoint, and therefore the results of this work largely focus on the mathematics of regime attribution.

We then performed a set of stratospheric relaxation model experiments, selecting 20 cases from the ECMWF hindcasts in which there was strong, coherent ensemble support for an incorrect regime to dominate during weeks 3–4. The majority (14) of these cases featured U100 errors approximately equal to or greater than the MAE in either week 3 or 4 or both, suggesting a link to the erroneous tropospheric forecasts. We found that the stratospheric relaxation is not enough to eliminate the regime errors, but the relaxation does lead to shifts in the ensemble distribution of the regimes within each forecast indicating substantial movement within PC space (Fig. 7). The results also showed an overall 10%–20% improvement in the accuracy of the forecasts in terms of Euclidean distance error/RMSE, which was most consistent in cases where the stratospheric error was larger (Fig. 8).

Analysis of the transition vectors between the CTR and RLX forecasts in PC space provided insight into the effect of stratospheric relaxation in the space in which regimes are assigned. The results (Fig. 10) illustrated that stratospheric

relaxation generally moved the forecasts toward the ERA-Interim verification *and* in the direction of that expected from the theory, while statistically nudging the CTR ensembles by the corresponding stratospheric perturbation vector also generally moved the forecasts toward the verification. For $|\Delta U| > \sim 3 \text{ m s}^{-1}$, this effect was particularly pronounced. Consequently, the model experiments support the proposed theory of which regime transitions may be possible solely because of changes to the stratospheric state (Fig. 5).

Overall, our results provide evidence that, all else being equal:

- The *average shift* of an ensemble of subseasonal North American weather regime forecasts in response to changes in the strength of the lower-stratospheric vortex is broadly generic and predictable.
- Correcting the stratospheric state leads to an improvement in the large-scale subseasonal tropospheric forecast over North America, but it does not necessarily correct the regime assignment (likely due to other sources of error).
- Some tropospheric regime states are more likely to change regime assignment for a given stratospheric perturbation than others. This arises due to the location of the regimes in PC space relative to the linear tropospheric response to the stratosphere.

We therefore propose that this vector-based approach can be used to identify, a priori, the regime forecast-verification scenarios in which lower-stratospheric errors are more likely to have played a substantial role—and thus toward understanding the overall contribution to subseasonal North American weather regime forecast accuracy. Further, it is possible that in certain circumstances when stratospheric uncertainty is dominant that the method could be used in real time to qualitatively interpret regime forecast uncertainty owing to stratospheric uncertainty. This approach is likely to be most useful 2–3 weeks before SSWs or strong vortex events, when abrupt forecast shifts (e.g., Lee et al. 2019a) are more likely due to the current predictability limit of these phenomena (Domeisen et al. 2020b). It may also be plausible to use the technique on-the-fly to linearly impose alternate regime “storylines” arising from a different stratospheric evolution without running additional dynamical forecasts.

Moreover, the dominantly linear and apparently generic response to the lower-stratospheric forcing on these time scales is somewhat similar to the long-lag response following SSWs in the model experiments of White et al. (2020). The idea that the tropospheric flow configuration following an imposed stratospheric change depends on the state of the troposphere is not a new idea (e.g., Gerber et al. 2009), but as a result, potential gains in subseasonal regime prediction skill from the stratosphere may be minimal if the tropospheric forecast otherwise drifts too far from the truth [also recently suggested by Charlton-Perez et al. (2021)]. This potential limitation is consistent with the regime forecasts remaining largely inaccurate even in cases where large lower-stratospheric errors were corrected, notwithstanding the imperfections of the model experiment.

Employing a stronger stratospheric nudging in the model experiments presented in this paper may produce greater improvement in the regime forecasts. On the other hand, constraining the prediction too strongly would exceed a

realistically achievable level of stratospheric forecast accuracy on these scales. It is also plausible that the nudging may have limited potential tropospheric forecast accuracy (when compared with a true perfect stratosphere forecast) by inducing unrealistic wave behavior or generation on the boundary of the nudging domain (Hitchcock et al. 2022). Also, model experiments with a greater horizontal and vertical resolution may also yield better results, with evidence supporting a link between increased resolution and better representation of modes of variability in S2S models (Quinting and Vitart 2019; Lee et al. 2020) and downward stratosphere–troposphere coupling (Kawatani et al. 2019). The 60-level model version used in the experiments performed here (limited by the resolution of ERA-Interim) is coarser than the 91-level model used operationally, suggesting there is scope for the impact of an improved stratospheric forecast to be greater in the operational model (and thus lead to more regime shifts).

Further, we have exclusively considered the effect of changes to the strength of the lower-stratospheric polar vortex defined through the zonal-mean zonal wind at 100 hPa and 60°N. A more complex analysis may incorporate the effects of wave propagation (Perlwitz and Harnik 2003; Kodera et al. 2008), vortex morphology (Cohen et al. 2021), or the representation of ozone chemistry (e.g., Oehrlein et al. 2020). While the use of zonal-mean quantities is motivated by annular modes, the approach can mask important subhemispheric variability such as localized wave reflection (e.g., Matthias and Kretschmer 2020).

A case-by-case analysis of the dynamics involved, including the interplay between stratospheric errors and other leading sources of subseasonal prediction (e.g., the Madden–Julian oscillation, which can act together with stratospheric variability; Schwartz and Garfinkel 2017; Barnes et al. 2019; Green and Furtado 2019) is a potentially fruitful avenue of future work. Moreover, using the proposed angular diagnostic to assess the tropospheric regime response to stratospheric perturbations across a much larger set of simulations (and in different geographic regions) will aid in understanding the robustness of the results of this study.

Acknowledgments. S.H.L. was funded by the Natural Environment Research Council (NERC) via the SCENARIO Doctoral Training Partnership (NE/L002566/1) at the University of Reading. S.J.W. was supported by the National Centre for Atmospheric Science, a NERC collaborative centre. This work is based on S2S data. S2S is a joint initiative of the World Weather Research Programme (WWRP) and the World Climate Research Programme (WCRP). The original S2S database is hosted at ECMWF as an extension of the TIGGE database. The authors thank Glenn Carver and Marcus Koehler at ECMWF for their support with OpenIFS and preparation of the initial conditions and relaxation data and three anonymous reviewers for their helpful comments on earlier versions of the manuscript.

Data availability statement. The ERA-Interim reanalysis and ECMWF hindcasts are available from the ECMWF website: <https://apps.ecmwf.int/datasets/>. OpenIFS experiment

data used in this study are available at <https://doi.org/10.5281/zenodo.4818044>. EOF and k -means clustering analysis were performed using the freely available Python packages “eofs” (Dawson 2016) and “scikit-learn” (Pedregosa et al. 2011), respectively.

REFERENCES

- Ambaum, M. H., B. J. Hoskins, and D. B. Stephenson, 2001: Arctic oscillation or North Atlantic oscillation? *J. Climate*, **14**, 3495–3507, [https://doi.org/10.1175/1520-0442\(2001\)014<3495:AOONAO>2.0.CO;2](https://doi.org/10.1175/1520-0442(2001)014<3495:AOONAO>2.0.CO;2).
- Amini, S., and D. M. Straus, 2019: Control of storminess over the Pacific and North America by circulation regimes. *Climate Dyn.*, **52**, 4749–4770, <https://doi.org/10.1007/s00382-018-4409-7>.
- Baldwin, M. P., and T. J. Dunkerton, 2001: Stratospheric harbingers of anomalous weather regimes. *Science*, **294**, 581–584, <https://doi.org/10.1126/science.1063315>.
- , and D. W. Thompson, 2009: A critical comparison of stratosphere–troposphere coupling indices. *Quart. J. Roy. Meteor. Soc.*, **135**, 1661–1672, <https://doi.org/10.1002/qj.479>.
- , D. B. Stephenson, D. W. Thompson, T. J. Dunkerton, A. J. Charlton, and A. O’Neill, 2003: Stratospheric memory and skill of extended-range weather forecasts. *Science*, **301**, 636–640, <https://doi.org/10.1126/science.1087143>.
- Barnes, E. A., S. M. Samarasinghe, I. Ebert-Uphoff, and J. C. Furtado, 2019: Tropospheric and stratospheric causal pathways between the MJO and NAO. *J. Geophys. Res. Atmos.*, **124**, 9356–9371, <https://doi.org/10.1029/2019JD031024>.
- Beerli, R., and C. M. Grams, 2019: Stratospheric modulation of the large-scale circulation in the Atlantic–European region and its implications for surface weather events. *Quart. J. Roy. Meteor. Soc.*, **145**, 3732–3750, <https://doi.org/10.1002/qj.3653>.
- Cassou, C., 2008: Intraseasonal interaction between the Madden–Julian oscillation and the North Atlantic Oscillation. *Nature*, **455**, 523–527, <https://doi.org/10.1038/nature07286>.
- Charlton, A. J., and L. M. Polvani, 2007: A new look at stratospheric sudden warmings. Part I: Climatology and modeling benchmarks. *J. Climate*, **20**, 449–469, <https://doi.org/10.1175/JCLI3996.1>.
- Charlton-Perez, A. J., L. Ferranti, and R. W. Lee, 2018: The influence of the stratospheric state on North Atlantic weather regimes. *Quart. J. Roy. Meteor. Soc.*, **144**, 1140–1151, <https://doi.org/10.1002/qj.3280>.
- , R. W. Aldridge, C. M. Grams, and R. Lee, 2019: Winter pressures on the UK health system dominated by the Greenland blocking weather regime. *Wea. Climate Extremes*, **25**, 100218, <https://doi.org/10.1016/j.wace.2019.100218>.
- , J. Bröcker, A. Y. Karpechko, S. H. Lee, M. Sigmond, and I. R. Simpson, 2021: A minimal model to diagnose the contribution of the stratosphere to tropospheric forecast skill. *J. Geophys. Res. Atmos.*, e2021JD035504, <https://doi.org/10.1029/2021JD035504>.
- Cohen, J., L. Agel, M. Barlow, C. I. Garfinkel, and I. White, 2021: Linking Arctic variability and change with extreme winter weather in the United States. *Science*, **373**, 1116–1121, <https://doi.org/10.1126/science.abi9167>.
- Dawson, A., 2016: eofs: A library for EOF analysis of meteorological, oceanographic, and climate data. *J. Open Res. Softw.*, **4**, e14, <https://doi.org/10.5334/jors.122>.
- Dee, D. P., and Coauthors, 2011: The ERA-Interim reanalysis: Configuration and performance of the data assimilation

- system. *Quart. J. Roy. Meteor. Soc.*, **137**, 553–597, <https://doi.org/10.1002/qj.828>.
- Domeisen, D. I. V., C. M. Grams, and L. Papritz, 2020a: The role of North Atlantic–European weather regimes in the surface impact of sudden stratospheric warming events. *Wea. Climate Dyn.*, **1**, 373–388, <https://doi.org/10.5194/wcd-1-373-2020>.
- , and Coauthors, 2020b: The role of the stratosphere in sub-seasonal to seasonal prediction: 1. Predictability of the stratosphere. *J. Geophys. Res. Atmos.*, **125**, e2019JD030920, <https://doi.org/10.1029/2019JD030920>.
- , and Coauthors, 2020c: The role of the stratosphere in sub-seasonal to seasonal prediction: 2. Predictability arising from stratosphere–troposphere coupling. *J. Geophys. Res. Atmos.*, **125**, e2019JD030923, <https://doi.org/10.1029/2019JD030923>.
- Douville, H., 2009: Stratospheric polar vortex influence on Northern Hemisphere winter climate variability. *Geophys. Res. Lett.*, **36**, L18703, <https://doi.org/10.1029/2009GL039334>.
- Fabiano, F., V. L. Meccia, P. Davini, P. Ghinassi, and S. Corti, 2021: A regime view of future atmospheric circulation changes in northern mid-latitudes. *Wea. Climate Dyn.*, **2**, 163–180, <https://doi.org/10.5194/wcd-2-163-2021>.
- Falkena, S. K., J. deWiljes, A. Weisheimer, and T. G. Shepherd, 2020: Revisiting the identification of wintertime atmospheric circulation regimes in the Euro-Atlantic sector. *Quart. J. Roy. Meteor. Soc.*, **146**, 2801–2814, <https://doi.org/10.1002/qj.3818>.
- Ferranti, L., S. Corti, and M. Janousek, 2015: Flow-dependent verification of the ECMWF ensemble over the Euro-Atlantic sector. *Quart. J. Roy. Meteor. Soc.*, **141**, 916–924, <https://doi.org/10.1002/qj.2411>.
- Garrido-Perez, J. M., C. Ordóñez, D. Barriopedro, R. García-Herrera, and D. Paredes, 2020: Impact of weather regimes on wind power variability in Western Europe. *Appl. Energy*, **264**, 114731, <https://doi.org/10.1016/j.apenergy.2020.114731>.
- Gerber, E., C. Orbe, and L. M. Polvani, 2009: Stratospheric influence on the tropospheric circulation revealed by idealized ensemble forecasts. *Geophys. Res. Lett.*, **36**, L24801, <https://doi.org/10.1029/2009GL040913>.
- Grams, C. M., R. Beerli, S. Pfenninger, I. Staffell, and H. Wernli, 2017: Balancing Europe's windpower output through spatial deployment informed by weather regimes. *Nat. Climate Change*, **7**, 557–562, <https://doi.org/10.1038/nclimate3338>.
- Green, M. R., and J. C. Furtado, 2019: Evaluating the joint influence of the Madden–Julian oscillation and the stratospheric polar vortex on weather patterns in the Northern Hemisphere. *J. Geophys. Res. Atmos.*, **124**, 11 693–11 709, <https://doi.org/10.1029/2019JD030771>.
- Han, J., M. Kamber, and J. Pei, 2012: Getting to know your data. *Data Mining*, Elsevier, 39–82, <https://doi.org/10.1016/B978-0-12-381479-1.00002-2>.
- Hannachi, A., I. T. Jolliffe, and D. B. Stephenson, 2007: Empirical orthogonal functions and related techniques in atmospheric science: A review. *Int. J. Climatol.*, **27**, 1119–1152, <https://doi.org/10.1002/joc.1499>.
- Hitchcock, P., and I. R. Simpson, 2014: The downward influence of stratospheric sudden warmings. *J. Atmos. Sci.*, **71**, 3856–3876, <https://doi.org/10.1175/JAS-D-14-0012.1>.
- , T. G. Shepherd, and G. L. Manney, 2013: Statistical characterization of Arctic polar night jet oscillation events. *J. Climate*, **26**, 2096–2116, <https://doi.org/10.1175/JCLI-D-12-00202.1>.
- , and Coauthors, 2022: Stratospheric Nudging and Predictable Surface Impacts (SNAPSI): A protocol for investigating the role of the stratospheric polar vortex in subseasonal to seasonal forecasts. *Geosci. Model Dev. Discuss.*, <https://doi.org/10.5194/gmd-2021-394>.
- Huang, W. T. K., A. Charlton-Perez, R. W. Lee, R. Neal, C. Sarran, and T. Sun, 2020: Weather regimes and patterns associated with temperature-related excess mortality in the UK: A pathway to sub-seasonal risk forecasting. *Environ. Res. Lett.*, **15**, 124052, <https://doi.org/10.1088/1748-9326/abcbb>.
- Jeuken, A., P. Siegmund, L. Heijboer, J. Feichter, and L. Bengtsson, 1996: On the potential of assimilating meteorological analyses in a global climate model for the purpose of model validation. *J. Geophys. Res. Atmos.*, **101**, 16 939–16 950, <https://doi.org/10.1029/96JD01218>.
- Jung, T., M. Miller, and T. Palmer, 2010a: Diagnosing the origin of extended-range forecast errors. *Mon. Wea. Rev.*, **138**, 2434–2446, <https://doi.org/10.1175/2010MWR3255.1>.
- , T. Palmer, M. Rodwell, and S. Serrar, 2010b: Understanding the anomalously cold European winter of 2005/06 using relaxation experiments. *Mon. Wea. Rev.*, **138**, 3157–3174, <https://doi.org/10.1175/2010MWR3258.1>.
- Karpechko, A. Y., P. Hitchcock, D. H. Peters, and A. Schneiderit, 2017: Predictability of downward propagation of major sudden stratospheric warmings. *Quart. J. Roy. Meteor. Soc.*, **143**, 1459–1470, <https://doi.org/10.1002/qj.3017>.
- Kautz, L.-A., I. Polichtchouk, T. Birner, H. Garny, and J. G. Pinto, 2020: Enhanced extended-range predictability of the 2018 late-winter Eurasian cold spell due to the stratosphere. *Quart. J. Roy. Meteor. Soc.*, **146**, 1040–1055, <https://doi.org/10.1002/qj.3724>.
- Kawatani, Y., K. Hamilton, L. J. Gray, S. M. Osprey, S. Watanabe, and Y. Yamashita, 2019: The effects of a well-resolved stratosphere on the simulated boreal winter circulation in a climate model. *J. Atmos. Sci.*, **76**, 1203–1226, <https://doi.org/10.1175/JAS-D-18-0206.1>.
- Kodera, K., H. Mukougawa, and S. Itoh, 2008: Tropospheric impact of reflected planetary waves from the stratosphere. *Geophys. Res. Lett.*, **35**, L16806, <https://doi.org/10.1029/2008GL034575>.
- , —, P. Maury, M. Ueda, and C. Claud, 2016: Absorbing and reflecting sudden stratospheric warming events and their relationship with tropospheric circulation. *J. Geophys. Res. Atmos.*, **121**, 80–94, <https://doi.org/10.1002/2015JD023359>.
- Kolstad, E. W., C. O. Wulff, D. I. Domeisen, and T. Woollings, 2020: Tracing North Atlantic Oscillation forecast errors to stratospheric origins. *J. Climate*, **33**, 9145–9157, <https://doi.org/10.1175/JCLI-D-20-0270.1>.
- Kretschmer, M., J. Cohen, V. Matthias, J. Runge, and D. Coumou, 2018: The different stratospheric influence on cold-extremes in Eurasia and North America. *npj Climate Atmos. Sci.*, **1**, 44, <https://doi.org/10.1038/s41612-018-0054-4>.
- Lee, S. H., A. Charlton-Perez, J. Furtado, and S. Woolnough, 2019a: Abrupt stratospheric vortex weakening associated with North Atlantic anticyclonic wave breaking. *J. Geophys. Res. Atmos.*, **124**, 8563–8575, <https://doi.org/10.1029/2019JD030940>.
- , J. C. Furtado, and A. J. Charlton-Perez, 2019b: Wintertime North American weather regimes and the Arctic stratospheric polar vortex. *Geophys. Res. Lett.*, **46**, 14 892–14 900, <https://doi.org/10.1029/2019GL085592>.
- , A. J. Charlton-Perez, J. C. Furtado, and S. J. Woolnough, 2020: Representation of the Scandinavia–Greenland pattern and its relationship with the polar vortex in S2S forecast models. *Quart. J. Roy. Meteor. Soc.*, **146**, 4083–4098, <https://doi.org/10.1002/qj.3892>.
- Leutbecher, M., and Coauthors, 2017: Stochastic representations of model uncertainties at ECMWF: State of the art and

- future vision. *Quart. J. Roy. Meteor. Soc.*, **143**, 2315–2339, <https://doi.org/10.1002/qj.3094>.
- Liang, Y.-C., J.-Y. Yu, E. S. Saltzman, and F. Wang, 2017: Linking the tropical Northern Hemisphere pattern to the Pacific warm blob and Atlantic cold blob. *J. Climate*, **30**, 9041–9057, <https://doi.org/10.1175/JCLI-D-17-0149.1>.
- Limpasuvan, V., D. L. Hartmann, D. W. Thompson, K. Jeev, and Y. L. Yung, 2005: Stratosphere–troposphere evolution during polar vortex intensification. *J. Geophys. Res. Atmos.*, **110**, D24101, <https://doi.org/10.1029/2005JD006302>.
- Magnusson, L., 2017: Diagnostic methods for understanding the origin of forecast errors. *Quart. J. Roy. Meteor. Soc.*, **143**, 2129–2142, <https://doi.org/10.1002/qj.3072>.
- Mariotti, A., and Coauthors, 2020: Windows of opportunity for skillful forecasts subseasonal to seasonal and beyond. *Bull. Amer. Meteor. Soc.*, **101**, E608–E625, <https://doi.org/10.1175/BAMS-D-18-0326.1>.
- Matsueda, M., and T. Palmer, 2018: Estimates of flow-dependent predictability of wintertime Euro-Atlantic weather regimes in medium-range forecasts. *Quart. J. Roy. Meteor. Soc.*, **144**, 1012–1027, <https://doi.org/10.1002/qj.3265>.
- Matthias, V., and M. Kretschmer, 2020: The influence of stratospheric wave reflection on North American cold spells. *Mon. Wea. Rev.*, **148**, 1675–1690, <https://doi.org/10.1175/MWR-D-19-0339.1>.
- Maycock, A. C., and P. Hitchcock, 2015: Do split and displacement sudden stratospheric warmings have different annular mode signatures? *Geophys. Res. Lett.*, **42**, 10943–10951, <https://doi.org/10.1002/2015GL066754>.
- , G. I. Masukwedza, P. Hitchcock, and I. R. Simpson, 2020: A regime perspective on the North Atlantic eddy-driven jet response to sudden stratospheric warmings. *J. Climate*, **33**, 3901–3917, <https://doi.org/10.1175/JCLI-D-19-0702.1>.
- Michelangeli, P.-A., R. Vautard, and B. Legras, 1995: Weather regimes: Recurrence and quasi stationarity. *J. Atmos. Sci.*, **52**, 1237–1256, [https://doi.org/10.1175/1520-0469\(1995\)052<1237:WRRAOQS>2.0.CO;2](https://doi.org/10.1175/1520-0469(1995)052<1237:WRRAOQS>2.0.CO;2).
- Mo, K. C., and R. E. Livezey, 1986: Tropical–extratropical geopotential height teleconnections during the Northern Hemisphere winter. *Mon. Wea. Rev.*, **114**, 2488–2515, [https://doi.org/10.1175/1520-0493\(1986\)114<2488:TEGHTD>2.0.CO;2](https://doi.org/10.1175/1520-0493(1986)114<2488:TEGHTD>2.0.CO;2).
- North, G. R., T. L. Bell, R. F. Cahalan, and F. J. Moeng, 1982: Sampling errors in the estimation of empirical orthogonal functions. *Mon. Wea. Rev.*, **110**, 699–706, [https://doi.org/10.1175/1520-0493\(1982\)110<0699:SEITEO>2.0.CO;2](https://doi.org/10.1175/1520-0493(1982)110<0699:SEITEO>2.0.CO;2).
- Oehrlein, J., G. Chiodo, and L. M. Polvani, 2020: The effect of interactive ozone chemistry on weak and strong stratospheric polar vortex events. *Atmos. Chem. Phys.*, **20**, 10531–10544, <https://doi.org/10.5194/acp-20-10531-2020>.
- Pedregosa, F., and Coauthors, 2011: Scikit-learn: Machine learning in Python. *J. Mach. Learn. Res.*, **12**, 2825–2830, <https://doi.org/10.48550/arXiv.1201.0490>.
- Pperlwitz, J., and N. Harnik, 2003: Observational evidence of a stratospheric influence on the troposphere by planetary wave reflection. *J. Climate*, **16**, 3011–3026, [https://doi.org/10.1175/1520-0442\(2003\)016<3011:OEOASI>2.0.CO;2](https://doi.org/10.1175/1520-0442(2003)016<3011:OEOASI>2.0.CO;2).
- Quinting, J., and F. Vitart, 2019: Representation of synoptic-scale Rossby wave packets and blocking in the S2S prediction project database. *Geophys. Res. Lett.*, **46**, 1070–1078, <https://doi.org/10.1029/2018GL081381>.
- Rex, D. F., 1951: The effect of Atlantic blocking action upon European climate. *Tellus*, **3**, 100–112, <https://doi.org/10.3402/tellusa.v3i2.8617>.
- Robertson, A. W., and M. Ghil, 1999: Large-scale weather regimes and local climate over the western United States. *J. Climate*, **12**, 1796–1813, [https://doi.org/10.1175/1520-0442\(1999\)012<1796:LSWRAL>2.0.CO;2](https://doi.org/10.1175/1520-0442(1999)012<1796:LSWRAL>2.0.CO;2).
- , N. Vigaud, J. Yuan, and M. K. Tippett, 2020: Toward identifying subseasonal forecasts of opportunity using North American weather regimes. *Mon. Wea. Rev.*, **148**, 1861–1875, <https://doi.org/10.1175/MWR-D-19-0285.1>.
- Runde, T., M. Dameris, H. Garny, and D. Kinnison, 2016: Classification of stratospheric extreme events according to their downward propagation to the troposphere. *Geophys. Res. Lett.*, **43**, 6665–6672, <https://doi.org/10.1002/2016GL069569>.
- Schwartz, C., and C. I. Garfinkel, 2017: Relative roles of the MJO and stratospheric variability in North Atlantic and European winter climate. *J. Geophys. Res. Atmos.*, **122**, 4184–4201, <https://doi.org/10.1002/2016JD025829>.
- Son, S.-W., H. Kim, K. Song, S.-W. Kim, P. Martineau, Y.-K. Hyun, and Y. Kim, 2020: Extratropical prediction skill of the Subseasonal-to-Seasonal (S2S) prediction models. *J. Geophys. Res. Atmos.*, **125**, e2019JD031273, <https://doi.org/10.1029/2019JD031273>.
- Straus, D. M., S. Corti, and F. Molteni, 2007: Circulation regimes: Chaotic variability versus SST-forced predictability. *J. Climate*, **20**, 2251–2272, <https://doi.org/10.1175/JCLI4070.1>.
- Thompson, D. W., and J. M. Wallace, 1998: The Arctic Oscillation signature in the wintertime geopotential height and temperature fields. *Geophys. Res. Lett.*, **25**, 1297–1300, <https://doi.org/10.1029/98GL00950>.
- Tripathi, O. P., A. Charlton-Perez, M. Sigmond, and F. Vitart, 2015: Enhanced long-range forecast skill in boreal winter following stratospheric strong vortex conditions. *Environ. Res. Lett.*, **10**, 104007, <https://doi.org/10.1088/1748-9326/10/10/104007>.
- van der Wiel, K., H. C. Bloomfield, R. W. Lee, L. P. Stoop, R. Blackport, J. A. Screen, and F. M. Selten, 2019: The influence of weather regimes on European renewable energy production and demand. *Environ. Res. Lett.*, **14**, 094010, <https://doi.org/10.1088/1748-9326/ab38d3>.
- Vautard, R., 1990: Multiple weather regimes over the North Atlantic: Analysis of precursors and successors. *Mon. Wea. Rev.*, **118**, 2056–2081, [https://doi.org/10.1175/1520-0493\(1990\)118<2056:MWROTN>2.0.CO;2](https://doi.org/10.1175/1520-0493(1990)118<2056:MWROTN>2.0.CO;2).
- Vigaud, N., A. W. Robertson, and M. K. Tippett, 2018: Predictability of recurrent weather regimes over North America during winter from submonthly reforecasts. *Mon. Wea. Rev.*, **146**, 2559–2577, <https://doi.org/10.1175/MWR-D-18-0058.1>.
- Wallace, J. M., and D. S. Gutzler, 1981: Teleconnections in the geopotential height field during the Northern Hemisphere winter. *Mon. Wea. Rev.*, **109**, 784–812, [https://doi.org/10.1175/1520-0493\(1981\)109<0784:TITGHF>2.0.CO;2](https://doi.org/10.1175/1520-0493(1981)109<0784:TITGHF>2.0.CO;2).
- Wang, S.-Y., L. Hipps, R. R. Gillies, and J.-H. Yoon, 2014: Probable causes of the abnormal ridge accompanying the 2013–2014 California drought: ENSO precursor and anthropogenic warming footprint. *Geophys. Res. Lett.*, **41**, 3220–3226, <https://doi.org/10.1002/2014GL059748>.
- Waugh, D. W., A. H. Sobel, and L. M. Polvani, 2017: What is the polar vortex and how does it influence weather? *Bull. Amer. Meteor. Soc.*, **98**, 37–44, <https://doi.org/10.1175/BAMS-D-15-00212.1>.
- White, C. J., and Coauthors, 2017: Potential applications of subseasonal-to-seasonal (S2S) predictions. *Meteor. Appl.*, **24**, 315–325, <https://doi.org/10.1002/met.1654>.

- White, I. P., C. I. Garfinkel, E. P. Gerber, M. Jucker, V. Aquila, and L. D. Oman, 2019: The downward influence of sudden stratospheric warmings: Association with tropospheric precursors. *J. Climate*, **32**, 85–108, <https://doi.org/10.1175/JCLI-D-18-0053.1>.
- , —, —, —, P. Hitchcock, and J. Rao, 2020: The generic nature of the tropospheric response to sudden stratospheric warmings. *J. Climate*, **33**, 5589–5610, <https://doi.org/10.1175/JCLI-D-19-0697.1>.
- Wilks, D., 2019: *Statistical Methods in the Atmospheric Sciences*. Elsevier, 818 pp.
- Yu, B., and X. Zhang, 2015: A physical analysis of the severe 2013/2014 cold winter in North America. *J. Geophys. Res. Atmos.*, **120**, 10 149–10 165, <https://doi.org/10.1002/2015JD023116>.